Proceedings of the ASME 2022
Pressure Vessels & Piping Conference
PVP2022
July 17-22, 2022, Las Vegas, NV, USA

PVP2022-81492

STRAIN-LIFE PERFORMANCE IN HYDROGEN OF A DOT PRESSURE VESSEL STEEL

May L. Martin[1], Peter E. Bradley[1], Damian Lauria[1], Robert L. Amaro[2], Matthew Connolly[1], Andrew J. Slifka[1]

[1]National Institute of Standards and Technology, Boulder, CO
[2]Advanced Materials Testing & Technologies, Cropwell, AL

ABSTRACT

Strain-life testing of a 4130 pressure vessel steel was conducted in air and in a high-pressure gaseous-hydrogen environment. Hydrogen causes an order of magnitude decrease in lifetime compared to in-air performance at the same strain-amplitudes. This decrease in lifetime in hydrogen is accompanied by various effects, such as a shift in the cyclic stress-strain curve, different influences on the elastic and plastic components of the strain-life data, and a distinct difference in the evolution of the microstructural texture prior to failure. For comparison, preliminary data from testing of a higher strength pressure vessel steel is presented, showing a difference in elastic/plastic partitioning may be accompanied by a difference in reduction in lifetime due to hydrogen.

Keywords: Hydrogen, Strain-life, Fatigue

1. INTRODUCTION

The drive for less expensive and lighter weight pressure vessels tends towards a desire for higher strength steels. For hydrogen gas storage, this directly conflicts with the trend of higher strength steels having a higher susceptibility to hydrogen embrittlement. This conflict has had a detrimental effect on the development of newer steels for hydrogen gas pressure vessel service, though recent studies have suggested that there may be reason to hope that different microstructures could defy this high-strength trend.

There are many test methods which can be used for the determination of lifetime of a structure due to cyclic loading, but two methods that directly determine lifetime over a range of cyclic loading conditions are stress-life and strain-life testing. For structures where the expected lifetime is on the lower end, such as below 100,000 cycles, strain-controlled testing is traditionally used, whereas stress-controlled testing is more commonly done when high-cycle fatigue damage response is desired. Data from either of these lifetime-testing techniques includes information on crack initiation and load-history-dependent damage response. For the development of models to describe the full damage response of a class of steels, strain-life testing provides a rich dataset. When the damage response is to be compared between the response in air or another inert environment to that of the response in hydrogen or some other chemically-active species, strain-controlled data can be used to great effect to probe differences in damage behavior including mechanistic differences. Typically, fatigue lifetimes are found to be drastically reduced in hydrogen gas, particularly for ferritic steels [1-4]. Another advantage is that strain-life testing reveals, with higher sensitivities, the effects of hydrogen on mechanical response. For this work, a pressure vessel steel that had seen hydrogen gas service was measured for comparison to previous measurements of the same steel in air [5]. The strain-life tests were performed at room temperature and 18 MPa hydrogen gas pressure over a range of strain amplitudes from 0.0021 to 0.025.

2. MATERIALS AND METHODS

2.1 Materials and sample geometry

The material tested was from a 4130 steel pressure vessel which had been in hydrogen service for 3 years, with a maximum in-service pressure of 41 MPa (6000 psi). The cylinder had an outer diameter of 230 mm (9 in.) and a wall thickness of 16.5 mm (0.65 in.). Chemical analysis results of the steel are given in Table 1. The 0.2% offset yield strength of the material is 696 ± 17 MPa, Young's modulus is 213 ± 8 GPa, and the ultimate tensile strength is 793 ± 12 MPa. This steel consists of a ferritic/martensitic microstructure with clear microstructural banding perpendicular to the through-thickness direction, Figure 1. This is similar to a rolled microstructure, as the steel

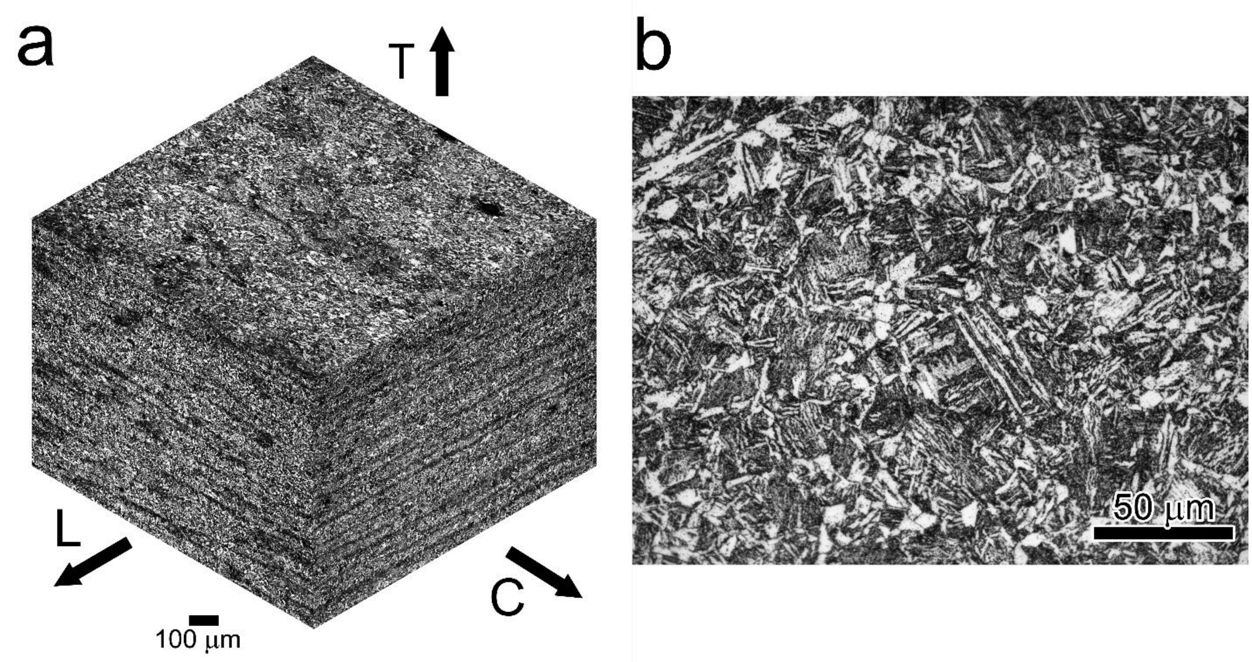

FIGURE 1: A) OPTICAL MICROGRAPH COMPOSITE OF REPRESENTATIVE MICROSTRUCTURE IN THE THREE CHARACTERISTIC PLANES (PERPENDICULAR TO THE L-LONGITUDINAL DIRECTION, THE C-CIRCUMFERENTIAL DIRECTION, AND THE T-THROUGH-THICKNESS DIRECTION. LIGHTER AREAS ARE COMPOSED PRIMARILY OF FERRITE GRAINS, WHILE DARKER AREAS ARE PRIMARILY MARTENSITE. B) HIGHER MAGNIFICATION IMAGE OF PLANE PERPENDICULAR TO LONGITUDINAL (L) DIRECTION.

TABLE 1: CHEMICAL COMPOSITION OF 4130 STEEL IN MASS PERCENT.

Fe	Cr	Mn	C	Si	Mo	S	P
97.749	1.03	0.5	0.32	0.21	0.17	0.01	0.011

underwent a hot drawing process when forming the cylinder. The grain size, as calculated from orientation mapping, is 3.1 ± 1.0 µm, which is likely an average of the martensite packet size and the ferrite grain size.

2.2 Mechanical testing set-up

Strain-life testing in hydrogen was conducted in 18 MPa hydrogen gas, following ASTM E606 [6], and compared to results from testing in air [5]. These hydrogen experiments were conducted in a high-pressure chamber described previously [7], with specific modifications, such as a compression clevis, described in [8] to allow large compressive loads, and ensure proper alignment of the load train. For strain-life testing, the procedure, by necessity is strain-controlled. Two strain gages, placed 90-120 ° apart, were used; one is the measurement/control gage, while the other is used to detect bending by the degree of deviation between the two strain measurements.

A strain-life test begins in either the tensile or compressive direction; our tests begin in the tensile direction. Tests in hydrogen were conducted at a constant strain rate of 0.002 /s, such that the highest test frequency is 1 Hz. To clarify, depending upon the strain amplitude applied, the frequency does vary by test (strain rate = strain amplitude*frequency).

Specimens were machined from the pressure vessel walls with the tensile axis aligned along either the longitudinal (L) or the circumferential/transverse (C) direction. A cylindrical dog-bone shaped configuration was chosen based upon ASTM standard criteria [6], but modified to accommodate limitations due to the pressure vessel size. Samples had a gage length of 22.23 mm (0.875 in) and a gage diameter of 6.35 mm (0.25 in), Figure 2.

2.3 Microstructural analysis

Samples were sectioned after mechanical testing to expose the cross-section of gage section approximately 3 mm from the crack (if visible) or as close as possible to the center of the gage length. The section was mounted in conductive epoxy and polished to a mirror finish. Electron back-scattered diffraction

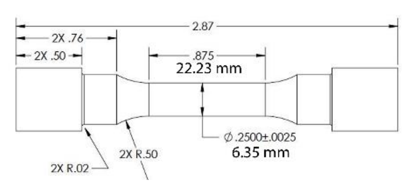

FIGURE 2: SCHEMATIC OF STRAIN-LIFE SPECIMENS. DIMENSIONS ARE IN INCHES UNLESS OTHERWISE INDICATED.

(EBSD) was conducted in a scanning electron microscope (SEM) operated at 30 kV. Scans were taken from the approximate center of the cross-section, and were 150 x 150 µm in size with 0.25 µm steps. Due to the tempered nature of the martensite, all points were indexed as ferrite.

3. RESULTS AND DISCUSSION

3.1 Strain-life testing

Fully-reversed strain-life testing produces hysteretic behavior, with softening in the case of this steel, Figure 3. As these tests begin in the tensile direction, the behavior at first is similar to a tensile test: linear elastic regime, followed by plastic yielding. As the strain is removed, the stress falls off linearly, again following a line with slope based on the elastic modulus. As the strain becomes compressive, plastic behavior resumes, and the curve bends over until the maximum compressive strain is achieved, at which point the process repeats in reverse. This material softens, which means that the maximum stress achieved decreases with subsequent cycles. As shown in Figure 3, this happens rapidly at first, then stabilizes as the test continues. In the stable regime, the maximum load as a function of cycle number follows a linear function, though the slope may not be zero. But as can be seen by the minimal differences between the hysteresis curves of Cycle 500 and Cycle 616 in Figure 3, once stable, the change in supported load is minimal. Once a crack forms in the sample, the load carried by the sample drops precipitously and failure occurs rapidly.

As can be seen in Figure 1, the two in-plane directions show similar microstructures. Samples taken from the longitudinal direction and the circumferential/transverse direction behaved similarly when subjected to identical strain amplitudes, Figure 4. There is a factor of two difference in the strain-life, but as with all fatigue-based failures, there is a large degree of statistical randomness to the initiation of failure. The location of flaws or inclusions in the material can have significant influence over the initiation of failure. Order of magnitude differences in lifetime are considered different, while factors of 2 are considered within the same decade of behavior, due to uncertainties in the lifetime. ASTM standard E606 reports within-laboratory uncertainties for tests targeting 1000 cycles producing an acceptable range of 700 to 1300 cycles [6], roughly a factor of two range. As can be seen in Figure 4a), the stabilized hysteresis curves are identical, so the material's cyclic response is the same in the two directions. Likewise, the reduction in maximum stress behavior is identical, when the difference in lifetime is taken into account, Figure 4b). This is a stronger support of similarity of the material's response

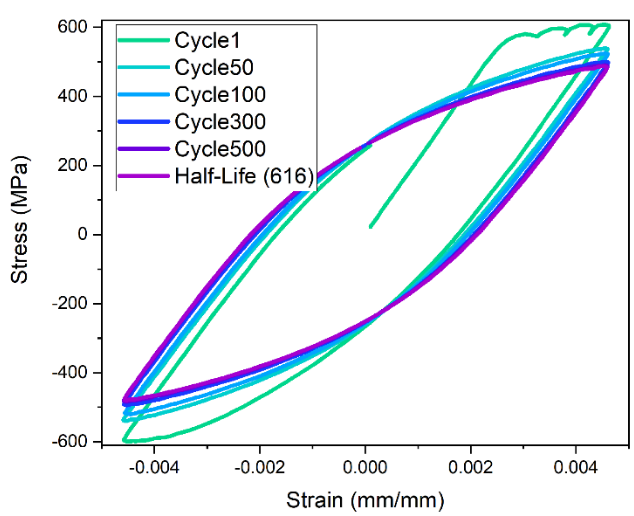

FIGURE 3: EVOLUTION OF THE STRESS-STRAIN HYSTERESIS CURVE IN 18 MPa H_2 AS A FUNCTION OF CYCLE NUMBER. "HALF-LIFE" IS HALF THE NUMBER OF CYCLES OF FAILURE AND IS ALSO CONSIDERED THE "STABILIZED CYCLE". NOTE VERY LITTLE CHANGE BETWEEN THE CYCLE 500 CURVE AND THE HALF-LIFE CURVE.

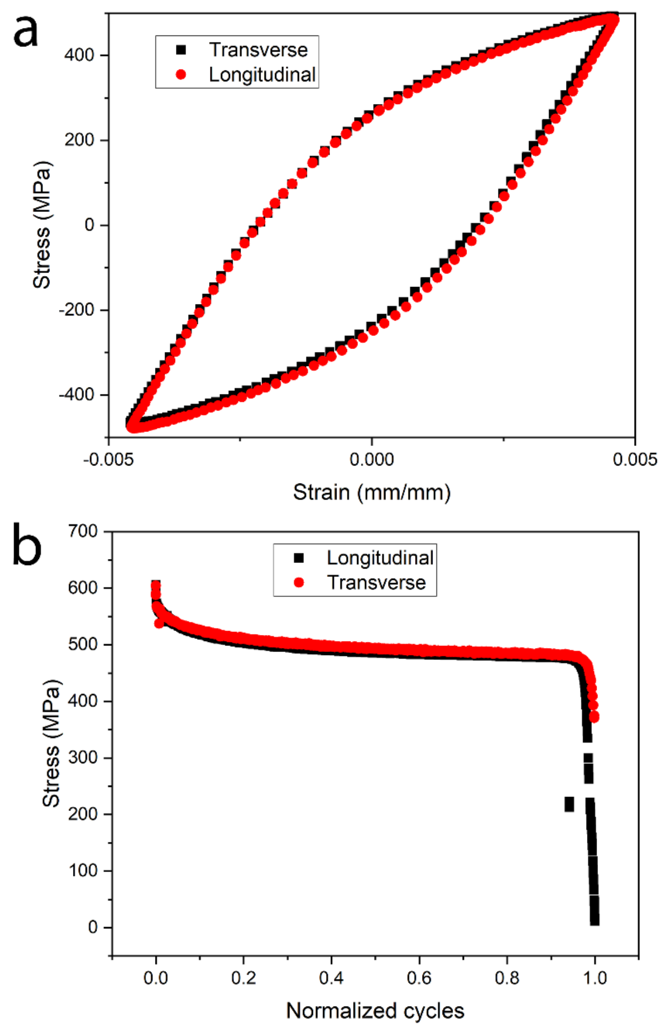

FIGURE 4: EFFECT OF ORIENTATION ON STRAIN-LIFE RESPONSE. DATA FROM TESTS OF A TRANSVERSE/ CIRCUMFERENTIAL SAMPLE AND OF A LONGITUDINAL SAMPLE BOTH LOADED AT A STRAIN-AMPLITUDE OF 0.0046 ARE COMPARED. A) STABILIZED HYSTERESIS LOOPS IN TRANSVERSE/CIRCUMFERENTIAL DIRECTION AND LONGITUDINAL DIRECTION ARE IDENTICAL. B) SOFTENING CURVES ARE IDENTICAL, AFTER ACCOUNTING FOR DIFFERENCE IN LIFETIME (NUMBER OF CYCLES TO FAILURE). THE LONGITUDINAL SAMPLE FAILED AFTER 1232 CYCLES, WHILE THE TRANSVERSE/ CIRCUMFERENTIAL SAMPLE FAILED AFTER 567 CYCLES.

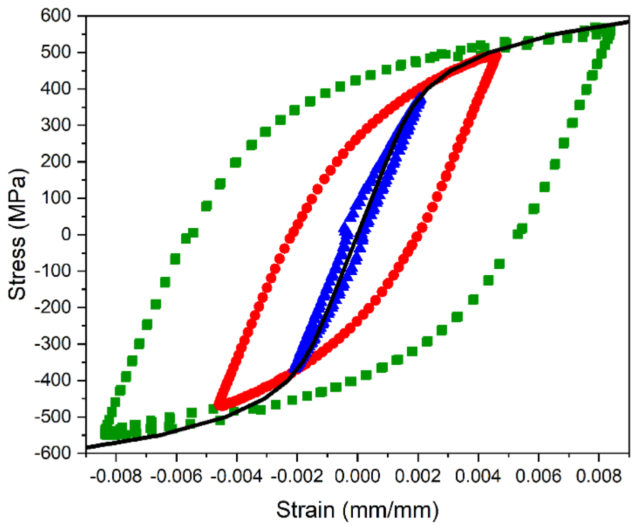

FIGURE 5: DIFFERENT STABILIZED HYSTERESIS CURVES FOR DIFFERENT APPLIED STRAIN AMPLITUDES IN HYDROGEN (ε_a = 0.0084, 0.0046, AND 0.0021). LINE DRAWN IS THE CYCLIC STRESS-STRAIN RELATIONSHIP.

in different crystallographic directions (with similar microstructures) than is available through tensile testing.

As the strain amplitude is varied, the hysteresis curves change, Figure 5. At smaller strain amplitudes (blue in the figure), where the material carries less stress, smaller hysteresis loops are formed. At larger strain amplitudes (green in the figure), as larger stresses are carried by the material and a greater percentage of the strain results in plasticity, the curves bend over at top due to yielding. It is also important to note that the increase in stress is not linear with the increase in strain amplitude, see curve in Figure 5. The cyclic stress-strain relationship is represented as:

$$\varepsilon = \frac{\sigma}{E} + \left(\frac{\sigma}{K'}\right)^{1/n'} \quad (1)$$

where ε is the strain amplitude, σ is the stress, E is the elastic modulus, and K´ and n´ are material specific parameters. The fitted values of K´ and n´ for the material tested in hydrogen are 1277 MPa and 0.18, respectively.

It is important to note that though Figures 3-5 show data from tests run in hydrogen gas, the trends observed (behavior of the hysteresis curve as the test progresses, similarity of behavior of longitudinal and transverse directions, and change in the hysteresis curve with strain amplitude) are also observed in air [9]. There are some differences in the exact trend (for softening and the cyclic stress-strain curve) and these will be discussed in this paper, but the general behavior with strain-life testing is the same.

3.2 The effect of hydrogen on strain-life testing

Strain-life testing ideally requires sampling of at least 3 decades of strain life (three orders of magnitude of cycles to failure). When comparing different environments, it is also desired to cover as much of the same strain-amplitude space as possible in both environments. As shown in Table 2, these two

TABLE 2: STRAIN-LIFE TESTING MATRIX FOR IN AIR AND IN HYDROGEN. DATA POINTS WITHIN THE SAME STRAIN-AMPLITUDE RANGE ARE SHADED IN BLUE.

Hydrogen environment		In air	
Strain Amplitude	Cycles to failure	Strain Amplitude	Cycles to failure
0.025	7	0.05	49
0.01	87	0.02	103
0.0092	93	0.01995	81
0.0084	131	0.0098	1631
0.0046	1232	0.0098	1381
0.0046	567	0.0093	1201
0.0035	2433	0.0042	16000
0.0021	27957	0.0042	20121

requirements were met, though there are areas at either extreme that do not have significant overlap due to the drastically reduced strain-life in hydrogen gas. While longer strain-life tests (lower applied strain amplitudes) could have been conducted in air, our study was focused on lifetimes relevant to pressure vessels, where lifetimes correspond to number of cycles that are expected during service. This data is graphically represented in Figure 6, with uncertainty ranges calculated according to ASTM E739 [10]. (Some of this data was presented in [8], however, due to miscommunication between the lab conducting in-air testing and the lab conducting hydrogen testing about $\Delta\varepsilon_a$ versus ε_a for the in-air and in-H_2 data, there is a factor of two error in the presented strain amplitude of the sets of data. This is corrected here. However, it is important to note that the strain-life data is sufficiently different between the two sets of data, that the conclusions of [8] still generally hold.) At the same applied strain amplitude, it can be seen that lifetimes are an order of magnitude shorter in hydrogen than in air.

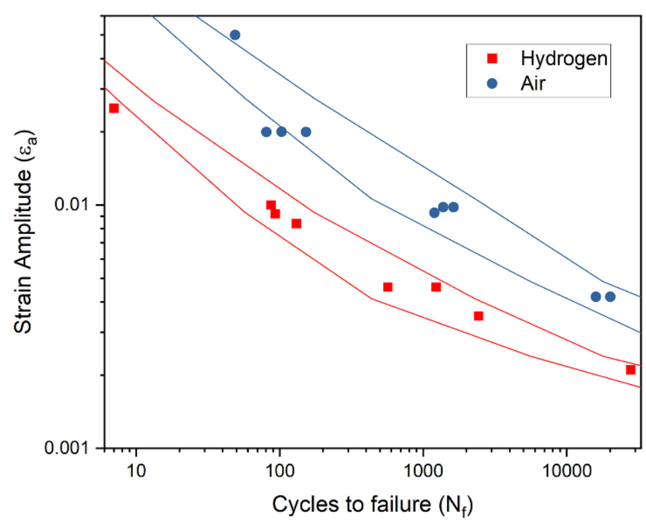

FIGURE 6: STRAIN-LIFE DATA IN AIR AND IN HYDROGEN. LINES INDICATE UNCERTAINTIES IN CYCLES TO FAILURE AS A FUNCTION OF APPLIED STRAIN AMPLITUDE, CALCULATED BY ASTM E739 [10].

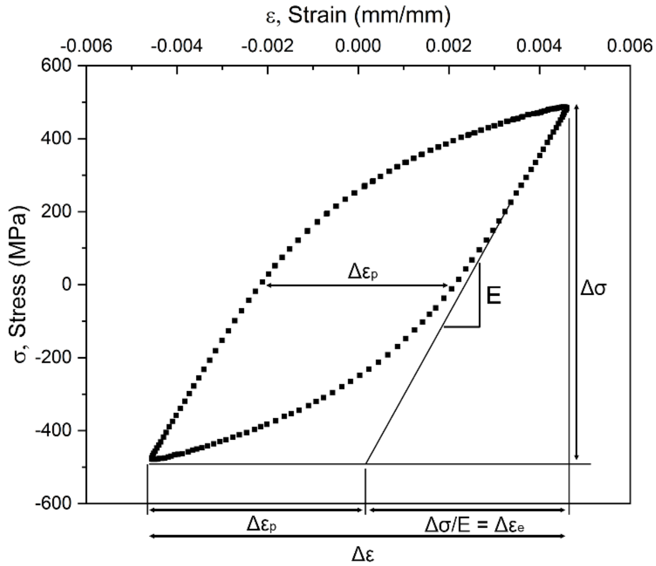

FIGURE 7: STABILIZED HYSTERESIS CURVE (CYCLE 616) OF HYDROGEN TEST AT STRAIN AMPLITUDE 0.0046 MARKED TO SHOW DIVISION INTO ELASTIC AND PLASTIC COMPONENTS.

Strain-life data can be broken into elastic and plastic components [11]. The strain amplitude is divided into elastic and plastic components determined from the stabilized curve, as shown in Figure 7. As can be seen in Figure 5, as the strain amplitude increases, the shape of the hysteresis curve changes, and the relative amounts of the elastic and plastic components change, with the plastic component becoming proportionally larger. The elastic component can be calculated based upon the stabilized stress amplitude (Δσ) and the measured effective elastic modulus (E). The plastic component of the strain amplitude is the remainder of the strain amplitude. There is a second method for determining the partitioning between elastic and plastic, which is also evident from Figure 7: the x-intercepts of the curve give plastic component of the strain amplitude, and the remainder of the strain amplitude is the elastic component. In general, the components calculated by the two methods from this dataset were within 10% of each other, with ¾ of the values within 5%. However, this second method has several advantages; the primary advantage is that the values can be easily taken from the data, rather than relying on a fitting of E. The elastic modulus is one of the least reliable variables to measure by bulk mechanical testing [12]. While most values (elastic and plastic) were fairly insensitive to variabilities in the value of E (10 % variation in E causes <5 % variation in strain component value), at the smallest strain amplitudes, where the plastic component was smallest, a variation in E of as small as 10 % causes nearly a 100 % change in the value of the plastic component of the strain amplitude. The second method of determining the x-intercepts of the curve is more reliable regardless of the strain amplitude.

This partitioning is shown in Figure 8a) where the in-hydrogen and in-air data are broken down into the elastic and plastic components. There it can be seen that the plastic components of the strain amplitude are small at lower strain

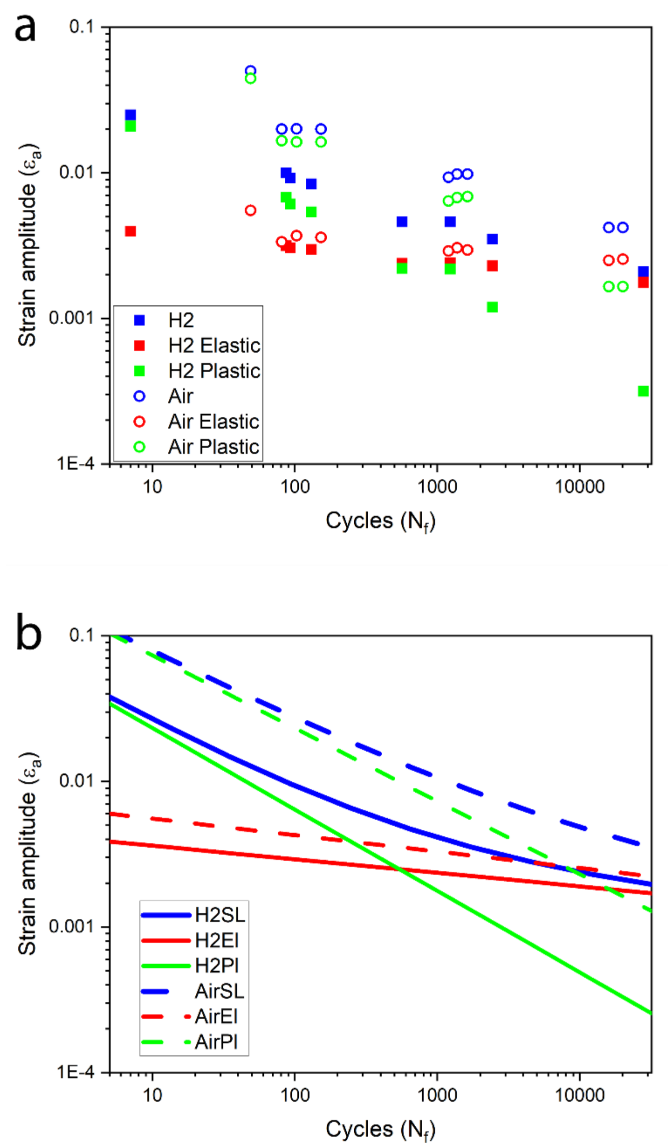

FIGURE 8: STRAIN-LIFE IN-AIR AND IN-H_2 DATA BROKEN INTO ELASTIC AND PLASTIC COMPONENTS. A) BREAKDOWN OF STRAIN-LIFE DATA INTO ELASTIC AND PLASTIC COMPONENTS. B) FITTED TRENDS OF DATA, INCLUDING ELASTIC AND PLASTIC COMPONENTS.

amplitudes (longer lifetimes) and are nearly the entirety of the strain amplitude at higher strain amplitudes (shorter lifetimes) in both air and hydrogen. Meanwhile, the elastic component is relatively constant, with only a slight decrease as a function of lifetime. The behavior of the two components is seen more clearly in Figure 8b), where the data is fitted to trendlines. While the full strain-life data follows a curve on a log-log plot, the elastic and plastic components follow linear trends on the same plot. The elastic trend is given by the Basquin relationship:

$$\frac{\Delta\varepsilon_{elastic}}{2} = \frac{\sigma_f'}{E}\left(2N_f\right)^b, \qquad (2)$$

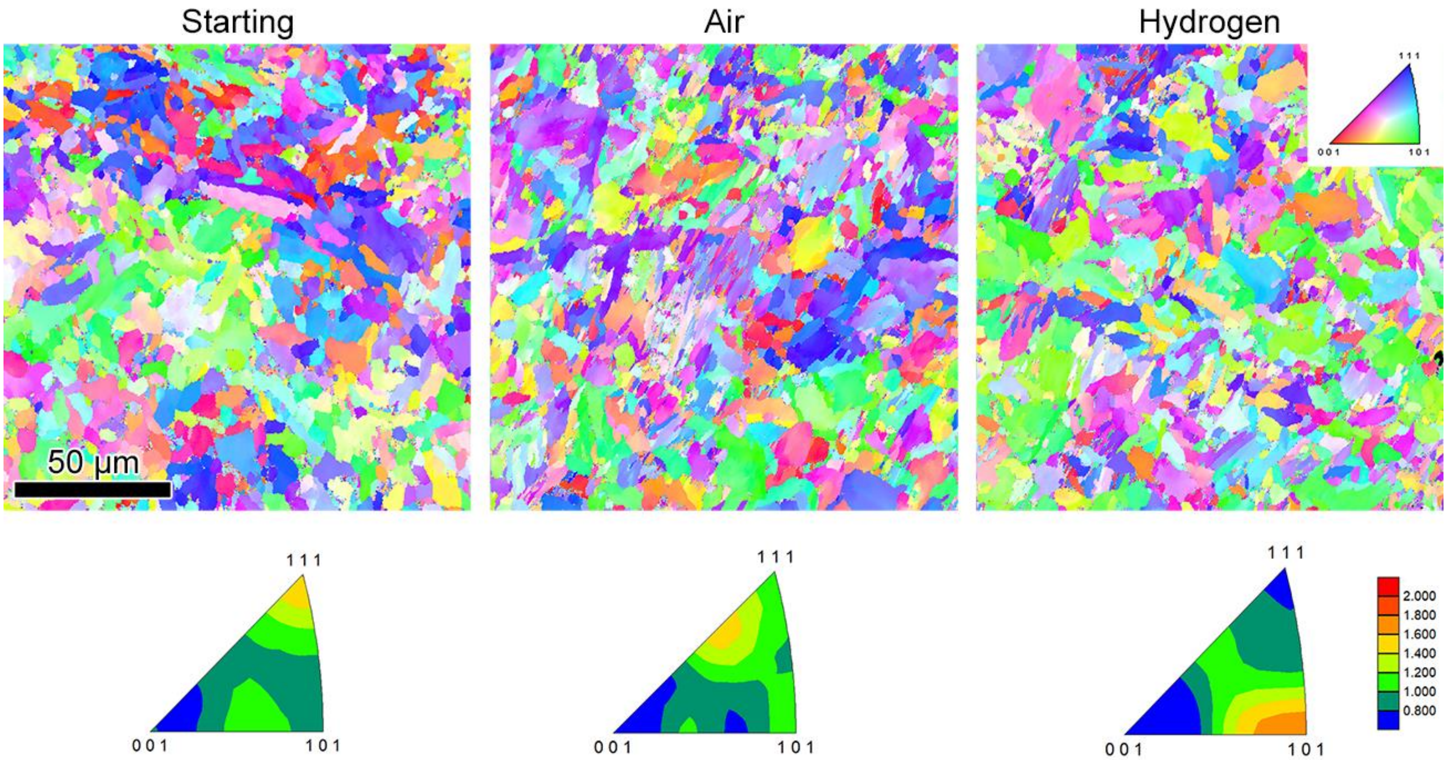

FIGURE 9: EBSD ANALYSIS OF STARTING MATERIAL (IN T DIRECTION), AIR SAMPLE AFTER STRAINING AT 0.0093 FOR 1201 CYCLES, AND IN HYDROGEN STRAINING AT 0.0092 FOR 93 CYCLES (BOTH CYCLED UNTIL "FAILURE"). INVERSE-POLE-FIGURE-COLORED MAPS SHOWN ON TOP, WITH INVERSE POLE FIGURES SHOWN BELOW. SCANS ARE 150 X150 µm WITH 0.25 µm STEPS.

where $\Delta\varepsilon_{elastic}$ is the elastic strain amplitude, σ_f' is the fatigue strength coefficient, E is the modulus of elasticity, and b is the fatigue strength exponent. The plastic trend is given by the Coffin-Manson relationship:

$$\frac{\Delta\varepsilon_{plastic}}{2} = \varepsilon_f'\left(2N_f\right)^c, \tag{3}$$

where $\Delta\varepsilon_{plastic}$ is the plastic strain amplitude, ε_f' is the fatigue ductility coefficient and c is the fatigue ductility exponent. The total strain life curve is the sum of the two components. Note that both equations frame the strain amplitude components as functions of $2N_f$, which is why it is tradition to plot strain-life as strain amplitude vs reversals (twice the cycles to failure). The fitted parameters for both in hydrogen and in air are given in Table 3.

TABLE 3: FIT PARAMETERS FOR BASQUIN AND COFFIN-MASON EQUATIONS IN HYDROGEN AND IN AIR. σ_f' HAS UNITS OF MPa, WHILE OTHER PARAMETERS ARE UNITLESS.

	σ_f'	b	ε_f'	c
Hydrogen	1003	-0.093	0.124	-0.559
Air	1634	-0.113	0.3296	-0.501

3.3 Microstructure evolution during strain-life testing

EBSD analysis of the cross-section taken ~3 mm below the generated crack gives some insight into the deformation processes going on in the material, Figure 9. The samples shown were cycled at the same strain amplitude (ε_a = 0.0093), though the sample in hydrogen failed at 1/10th the number of cycles of the sample cycled in air (93 vs 1201 cycles). Despite this drastic difference in lifetime, the sample cycled in hydrogen shows significantly more reorientation than that in air, suggesting an acceleration in deformation, beyond that required for failure in air. This is in contrast to the results shown in [8], wherein the hydrogen sample that had the same strain-life as the sample in air, but lower applied strain amplitude, showed less reorientation for what should have been similar amounts of damage. Note that at the same applied strain amplitude, the percentage of the strain amplitude that is considered "plastic" is the same, regardless of the environmental conditions. At the same strain-life, since the applied strain amplitude is less in hydrogen, the percentage that is considered "plastic" would be less as well. It is evident that hydrogen has an effect on the dislocation processes in the material, and that the effect is complicated.

3.3 High-strength steel comparison

While this paper has concentrated on the results of a "baseline" 4130 steel, to demonstrate some of the performance information that can be extracted from this sort of testing, preliminary results from a high-strength pressure vessel steel are compared against the baseline steel in Figure 10. This martensitic steel has a strength of 1100 MPa, which is above the "rule of thumb" cut-off of 950 MPa in strength for hydrogen usage. The samples were cut from a pressure vessel that was permitted for non-hydrogen applications, but never saw service, and due to the thinner walls of the vessel (10.92 mm/0.43 in or ~2/3 the thickness of the baseline material), these samples were significantly thinner than the baseline steel. However, care was taken to ensure the new sample design resulted in comparable results, accounting for factors such as grain size and distribution differences between the materials. Several successful tests were completed in air and in hydrogen, allowing the comparison shown in Figure 10.

Looking at the air data, it appears that this higher strength steel does not have quite the same performance as the baseline material, showing slightly lower lifetimes for the same applied strain amplitude. However, given the uncertainties in the strain-life ranges, and the limited number of data points for the high strength steel, there might not be a large difference in behavior. But, given that the higher strength steel was tempered to a lesser degree than the baseline steel, it would be unsurprising that it is more brittle in air.

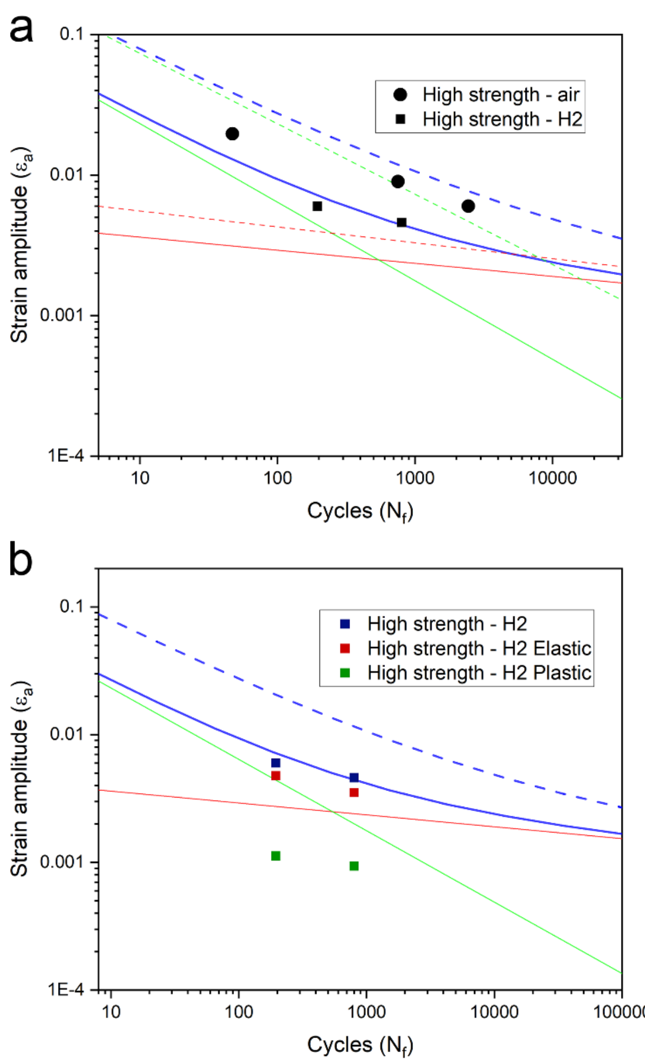

FIGURE 10: STRAIN-LIFE DATA OF "HIGH STRENGTH" STEEL OVERLAID ON 4130 STEEL DATA FROM FIGURE 8B). A) SHOWS THE PERFORMANCE OF THE HIGH STRENGTH STEEL IN AIR AND IN HYDROGEN COMPARED TO THE BASELINE STEEL TRENDS FROM FIGURE 8B). B) SHOWS THE HYDROGEN DATA PARTITIONED INTO ELASTIC AND PLASTIC COMPONENTS OVERLAID ON THE TRENDS IN HYDROGEN FOR THE BASELINE STEEL. THE BASELINE IN-AIR STRAIN-LIFE TREND IS PLOTTED FOR COMPARISON.

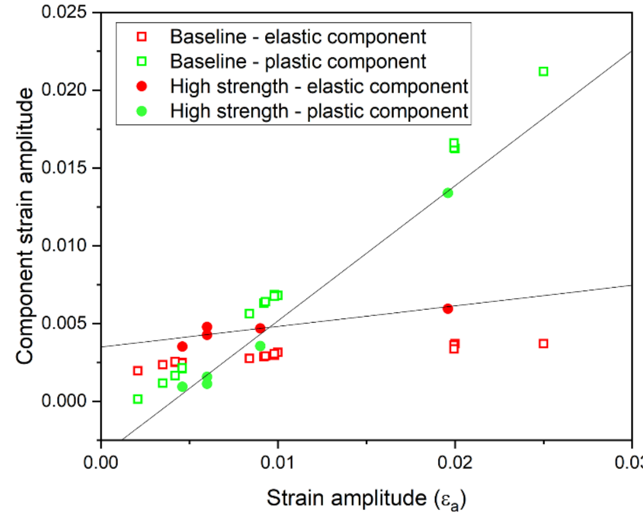

FIGURE 11: BREAKDOWN OF ELASTIC AND PLASTIC COMPONENTS OF THE STRAIN AMPLITUDE AS A FUNCTION OF THE STRAIN AMPLITUDE IN BASELINE (4130) STEEL AND "HIGH-STRENGTH" STEEL. NOTE HOW THE TWO MATERIALS FALL ON DIFFERENT, BUT NEARLY PARALLEL, LINES.

At first glance, the hydrogen data is promising: the hydrogen data from the high strength steel appears to be similar to the baseline steel, suggesting less of a relative reduction in lifetime for the high strength steel compared to the baseline steel. Looking at the partitioning, the response is dominated by the elastic response, with little plastic contribution, while this region comprises the cross-over from plastic to elastic dominated behavior for the baseline material. This difference in partitioning is even clearer when plotting the relative components ($\varepsilon_p/\varepsilon_a$ or $\varepsilon_e/\varepsilon_a$) vs the applied amplitude (ε_a), Figure 11. Here, all of the baseline steel data (in air and in hydrogen) falls along the same lines for the plastic component and elastic component. Likewise, all of the high strength steel data points lie along lines, with the plastic component significantly higher and the elastic component lower than in the baseline material.

By looking at the changes in the lifetime with applied strain, and especially looking at the partitioning between plastic and elastic components, the differences between materials' responses can be easily seen. This is even before using the concept of "damage" to model the differences in materials' response.

3.4 Discussion

Tensile testing of various geometries [13, 14], fatigue crack growth rate testing of various geometries [1, 3, 4], bending testing of various geometries [15, 16], and even high pressure torsion [17] have all been done in hydrogen, and are generally easier to conduct *in situ* than strain-life testing. What does loading in compression and determining lifetime add? To begin with, strain-life and stress-life testing are heavily used in industries like aerospace, where knowledge of lifetimes is often critical. Testing in the environment means that safety factors don't need to be added to account for the environment, as you have the data. Strain-life testing also incorporates crack nucleation due to the manner of testing, which is not the case for fatigue crack growth rate testing.

Understanding the effects that hydrogen can have on a material is critical: recent research has made it clear that the effect of hydrogen is not as simple as a simple reduction in ductility due to embrittlement. Hydrogen has many effects on the mechanical properties of structural metals (see reviews [18, 19]), many of which are competing in effects or concealed by other factors when looking at mechanical testing results. An example of this can be seen by looking at the literature trends in the yield point from tensile tests. Some studies suggest that the yield point increases with hydrogen, while others (such as the tensile results of the 4130 steel shown in Figure 12) show a decrease with hydrogen, and still others show a negligible change with environment due to uncertainties in the results [18]. The net result is that there is no conclusive evidence of hydrogen on the macroscopic yield point of steels, despite evidence of hydrogen's influence on the microscopic yielding of steels [20]. However, a clearer difference can be seen by comparing the cyclic stress-strain curves in air and in hydrogen (Figure 12). As shown in Figure 3 and Figure 5, the hysteresis behavior during strain-life settles from a first pull which closely resembles the tensile curve, as seen in Figure 12, to a stabilized curve and, from the extreme points of the stabilized curves generated at various applied strain amplitudes, a cyclic stress-strain curve can be fitted. As shown in Figure 12, the in-hydrogen curve is higher than the in-air curve due to less softening occurring in hydrogen than in air. Whether this is due to less softening occurring due to the abbreviated lifetime at the same strain-amplitudes, or whether hydrogen is influencing softening behaviors in other ways that are not globally observable is the focus of further investigation. But there is a clear trend to be seen, and unlike in tensile testing, there is more data behind the curve that can be probed for further insight.

While the presence of a hydrogen gas environment did have significant effect on the lifetime of this steel, it is worth noting that the effects on the many of the specific aspects of behavior during strain-life testing were more subtle. An increase in strain-amplitude leads to a decrease in strain-life, along a macroscopically similar curve as in air, though with a significant (order-of-magnitude) offset. The cyclic stress-strain curve followed the expected curve and is similar to the in-air curve. This ferritic/martensitic steel still displayed a significant amount of softening in hydrogen. And the directional dependence of mechanical behavior (or lack thereof) did not change in the presence of hydrogen. A first-look conclusion could be that hydrogen has a limited effect on the material, other than to promote failure initiation.

As mentioned above, the most immediately notable effect of hydrogen is the reduction in the lifetime, by 1-2 orders of magnitude at the same strain-amplitude as in air. The other way to view this data is that the same strain-life, or the same amount of damage, occurs at roughly half the strain amplitude in hydrogen that it does in air. While uncertainties in the lifetime are quite large, they are still smaller than the difference between

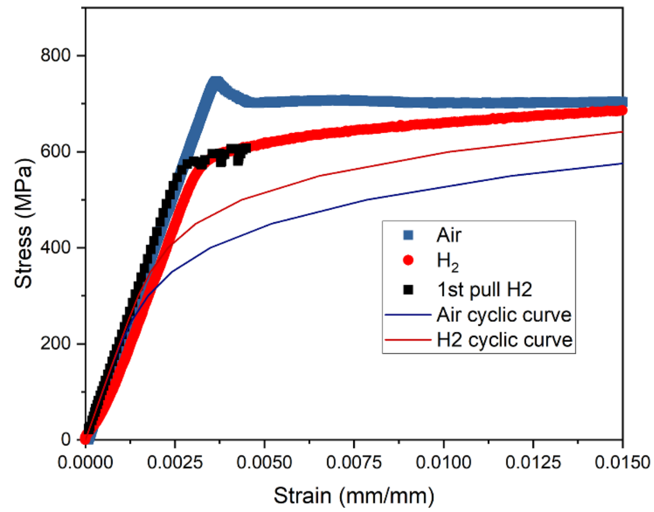

FIGURE 12: COMPARISON OF TENSILE CURVES (IN AIR AND IN H_2) AND THE CYCLIC STRESS-STRAIN CURVES (IN AIR AND IN H_2). FOR COMPARISON, THE FIRST PULL OF A TEST IN HYDROGEN IS ADDED; IT FOLLOWS CLOSELY THE TENSILE CURVE IN H_2.

the in-air and in-hydrogen trends, Figure 6; the order of magnitude difference is real. Looking at the results from a damage point of view, where similar strain-lives translates as similar levels of damage, it can be said that a similar level of damage is achieved in the material in hydrogen at half the strain amplitude that it takes in air. Hydrogen is accelerating the accumulation of damage.

Looking at the breakdown of the strain-life curves into elastic and plastic contributions reveals other differences in the response depending upon environment. While there are a 20% and a 10% difference in the slopes of the elastic and plastic contributions to strain-life curves in air and in hydrogen, these differences are sufficiently within the uncertainties of the measurements and fits such that the differences may be negligible. However, it is evident that the cross-over point, where elastic and plastic contributions trade which one is dominant, is different in air and in hydrogen. In hydrogen, the number of reversals where the cross-over point occurs is an order of magnitude smaller than where it occurs in air. Interestingly, it occurs at nearly the same applied strain amplitude in both environments. Over the range examined, the response in air is dominated by the plastic behavior until very low strain amplitudes/very long lifetimes. By contrast, the response in hydrogen is dominated by the elastic response at shorter lifetimes/higher strain amplitudes. Looking at the difference in the plastic and elastic strain-life curves in air and in hydrogen, plasticity appears more strongly affected by environment. However, the details of how hydrogen affects the plasticity to cause this change is not evident from this analysis of the data and will be the focus of further studies.

4. CONCLUSION

A 4130 martensitic/ferritic pressure vessel steel was strain-life tested in a hydrogen environment. Compared to the performance in air, the material showed an order of magnitude reduction in lifetime at the same applied strain amplitudes. While a simplistic approach to the data suggests that hydrogen has little effect other than a shortening of lifetime, there remains a wealth of information to still be garnered from the data. Other information such as the influence of hydrogen on the softening behavior, combined with the microstructural analysis suggests that the effect of hydrogen is very complicated and that extensive analysis of the strain-life data may provide further insight.

REFERENCES

[1] A.J. Slifka, E.S. Drexler, R.L. Amaro, L.E. Hayden, D.G. Stalheim, D.S. Lauria, N.W. Hrabe, Fatigue Measurement of Pipeline Steels for the Application of Transporting Gaseous Hydrogen1, Journal of Pressure Vessel Technology, 140 (2017).

[2] P.P. Darcis, J. McColskey, A. Lasseigne, T. Siewert, Hydrogen effects on fatigue crack growth rate in high strength pipeline steel, in: 2008 International hydrogen conference–effects of hydrogen on materials, September 7, 2008–September 10, 2008, ASM International Jackson (WY, United States), 2009, pp. 381-388.

[3] J.A. Ronevich, B.P. Somerday, C.W. San Marchi, Effects of microstructure banding on hydrogen assisted fatigue crack growth in X65 pipeline steels, International Journal of Fatigue, 82 (2016) 497-504.

[4] Y. Murakami, S. Matsuoka, Effect of hydrogen on fatigue crack growth of metals, Engineering Fracture Mechanics, 77 (2010) 1926-1940.

[5] C.P. Looney, Z.M. Hagan, M.J. Connolly, P.E. Bradley, A.J. Slifka, R.L. Amaro, Modelling the test methods used to determine material compatibility for hydrogen pressure vessel service, International Journal of Fatigue, 132 (2020) 105339.

[6] ASTM Standard E 606-04 E1 "Standard Practice for Strain-Controlled Fatigue Testing", 2004, A. International, West Conshohocken, PA.

[7] A.J. Slifka, E.S. Drexler, N.E. Nanninga, Y.S. Levy, J.D. McColskey, R.L. Amaro, A.E. Stevenson, Fatigue crack growth of two pipeline steels in a pressurized hydrogen environment, Corrosion Science, 78 (2014) 313-321.

[8] M.L. Martin, C. Looney, P. Bradley, D. Lauria, R. Amaro, A.J. Slifka, Unification of hydrogen-enhanced damage understanding through strain-life experiments for modeling, Engineering Fracture Mechanics, 216 (2019) 106504.

[9] C.P. Looney, Accumulated Inelastic Strain Based Damage Modeling of Pressure Vessel Steels in Air, in, Colorado School of Mines, 2018.

[10] ASTM E739-10 Standard Practice for Statistical Analysis of Linear or Linearized Stress-Life (S-N) and Strain-Life (ε-N) Fatigue Data, E739-10, 2015, ASTM International,

[11] N.E. Dowling, Mean stress effects in strain–life fatigue, 32 (2009) 1004-1019.

[12] J.D. Lord, R.M. Morrell, Elastic modulus measurement—obtaining reliable data from the tensile test, Metrologia, 47 (2010) S41-S49.

[13] M. Wang, E. Akiyama, K. Tsuzaki, Crosshead speed dependence of the notch tensile strength of a high strength steel in the presence of hydrogen, Scripta Materialia, 53 (2005) 713-718.

[14] L. Cho, P.E. Bradley, D.S. Lauria, M.J. Connolly, E.J. Seo, K.O. Findley, J.G. Speer, L. Golem, A.J. Slifka, Effects of hydrogen pressure and prior austenite grain size on the hydrogen embrittlement characteristics of a press-hardened martensitic steel, International Journal of Hydrogen Energy, 46 (2021) 24425-24439.

[15] M. Pinson, H. Springer, T. Depover, K. Verbeken, Qualification of the in-situ bending technique towards the evaluation of the hydrogen induced fracture mechanism of martensitic Fe–C steels, Materials Science and Engineering: A, 792 (2020) 139754.

[16] T. Ohmisawa, S. Uchiyama, M. Nagumo, Detection of hydrogen trap distribution in steel using a microprint technique, Journal of Alloys and Compounds, 356-357 (2003) 290-294.

[17] Y. Mine, Z. Horita, Y. Murakami, Effect of hydrogen on martensite formation in austenitic stainless steels in high-pressure torsion, Acta Materialia, 57 (2009) 2993-3002.

[18] M.L. Martin, M.J. Connolly, F.W. DelRio, A.J. Slifka, Hydrogen embrittlement in ferritic steels, Applied Physics Reviews, 7 (2020) 041301.

[19] R.P. Gangloff, B.P. Somerday, Gaseous hydrogen embrittlement of materials in energy technologies: the problem, its characterisation and effects on particular alloy classes, Elsevier, 2012.

[20] M.L. Martin, M. Dadfarnia, A. Nagao, S. Wang, P. Sofronis, Enumeration of the hydrogen-enhanced localized plasticity mechanism for hydrogen embrittlement in structural materials, Acta Materialia, 165 (2019) 734-750.